Normalized Difference Vegetation Index and Standard Precipitation Index Parameters to Monitor Drought at National Scale: The Case of Ethiopia

Getachew Berhan,[1] Tsegaye Tadesse,[2] Solomon Atnafu,[3] Shawndra Hill[4] and Yitaktu Tesfatsion[5]

Abstract

The main objective of this research was to characterize and identify drought incidence using both historic rainfall (RF) data and satellite-images. From the analysis of the relationships between average 12 months RF and NDVI, there were high R^2 values for rainy months. For the remaining dry months of the year, there were low relationships (with R^2 values of less than 0.5). We concluded that it is possible to use the near real-time MSG and historical NOAA AVHRR NDVI and Dev_NDVI data with some calibration and validation to identify and predict drought incidences. The outputs of this research can help decision makers to take appropriate actions to mitigate the adverse effects of drought.

Keywords: drought monitoring, NDVI, satellite image, SPI

[1] PhD Student, Addis Ababa University, Ethiopia, Tel: 251 911 638408, P.O.Box 1176, getachewb1@yahoo.com
[2] Asst. Professor, University of Nebraska-Lincoln, USA, ttadesse2@unl.edu
[3] Asst. Professor, Addis Ababa University, Ethiopia, satnafu@cs.aau.edu.et
[4] Asst. Professor, University of Pennsylvania, USA, shawndra@wharton.upenn.edu
[5] Senior Remote Sensing Expert, National Meteorological Agency, Ethiopia, yitaktut@gmail.com

Introduction

Frequent and severe drought has become one of the most important natural disasters in sub-Saharan Africa, especially in Ethiopia. The issue of drought monitoring has also received attention from experts and scientists. This is due to the fact that drought is one of the major causes of economic, social, and environmental crises (Tadesse *et al.*, 2008). Its effect is marked by the creation of uncertain agricultural economies in developing countries (UNEP, 2006).

Drought is defined as "the naturally occurring phenomenon that exists when precipitation has been significantly below normal recorded levels, causing serious hydrological imbalances that adversely affect land resource production systems" (UNCCD, 1999). Drought is also defined as a prolonged, abnormally dry period when there is not enough water for users' normal needs, resulting in extensive damage to crops and loss of yields (Wilhite, 2005). These definitions of drought are conceptual definitions and are the basis for the operational definition. The operational definition of drought focuses on identifying the beginning, end, spatial extent, and severity of the drought in a given region and it is based on scientific reasoning. The analysis is done using hydro-meteorological information and is beneficial in developing drought policies, early warning monitoring systems, mitigation strategies, and preparedness plans (Smakhtin and Hughes, 2004).

There are three types of drought: meteorological drought, agricultural drought, and hydrological drought (UNISDR, 2009). The definitions for these three drought types are given by UNISDR (2009). While meteorological drought is usually defined by a precipitation deficiency over a pre-determined period of time, agricultural drought is defined more commonly by the lack of soil water to support crop and forage growth than by the departure of normal precipitation over some specified period of time. Hydrological drought is normally defined by deficiencies in surface and subsurface water supplies relative to average conditions at various points in time through the seasons. These three types of drought gradually contribute

to socioeconomic drought, which is the anomaly in supply and demand for economic goods (such as water, livestock forage, hydroelectric power, etc.) that are dependent upon precipitation (UNISDR, 2009).

National Meteorological Agency of Ethiopia has attempted to collect and document the history of drought and its impact on various administrative regions of Ethiopia from different national and international documents. Accordingly, the analysis of the chronological events of Ethiopian drought has been divided into four parts (NMSA, 1996). The first one is from 253 B.C. (Before Christ) to A.D. (Anno Domini – "in the year of our lord"); during this period, one drought was reported in seven years' time. The second one is reported from A.D. to 1500 A.D. During this time there were devastating droughts known as "Asah", "Fassas" and "Higlah", which killed millions of lives. In this period, there were 177 droughts in the country, about one every nine years. The third period was from 1500 to 1900, and the information is relatively based on recorded data and, therefore, more reliable. From the 16th to the first half of the 20th century, ten, fourteen, twenty-one, sixteen, and eight droughts were reported, respectively, suggesting sixty-nine events in a period of 450 years. The two notorious droughts known as "Quachine" and "Kifuken", which devastated major areas of the country, were reported during this period. The fourth period (from 1950 to 1988) is well documented with scientific data. The analysis of the rainfall data during this period indicated 18 droughts in 38 years, suggesting the occurrence of drought every two years. The worst period appears to be the 1980s and the worst year is 1984 (NMSA, 1996).

In the analysis of drought, the onset, duration, and severity of droughts are often difficult to determine and the characteristics may vary significantly from one region to another (Rulinda *et al.,* 2010). In rainfall-dependent agriculture production areas, seasonal rainfall variability is inevitably reflected in both highly variable production levels and in the risk-averse livelihoods of local farmers (Cooper *et al.,* 2008).

The conventional approach to drought monitoring and early warning systems using ground-based data collection is tedious, time consuming, and difficult (Prasad *et al.,* 2007). In recent years, remote sensing data has been

used for monitoring agro-climatic conditions, the state of the agricultural fields, vegetation cover, and to estimate crop yield in various countries. In particular, the advanced very high resolution radiometer (AVHRR) NDVI data has been used in vegetation monitoring, crop yield assessment, and forecasting (Hayes *et al.*, 1982; Benedetti and Rossini, 1993; Quarmby *et al.*, 1993; Unganai and Kogan, 1998; Kogan *et al.*, 2003). The National Oceanic and Atmospheric Administration (NOAA) AVHRR-series satellite data provides a long-term record of NDVI data that can be used in the prediction of crop yield (Prasad *et al.*, 2007).

The other remote sensing data source for monitoring agro-climatic conditions is Meteosat Second Generation (MSG) satellite. MSG is the new European system of geostationary meteorological satellites together with the associated infrastructure. It was developed to succeed the highly successful series of original Meteosat satellites that served the meteorological community for over two decades since it was first launched in 1977 (EUMETSAT, 2005). The advanced Spinning Enhanced Visible and Infrared Imager (SEVIRI) radiometer onboard of the MSG series of geostationary satellites enables the Earth to be scanned in 12 spectral channels, from visible to thermal infrared, at 15-minute intervals. Each of the 12 channels has one or more specific applications, either when used alone or in conjunction with data from other channels.

From the climatologically data sources, Standard Precipitation Index (SPI) is the usual drought monitoring parameter. The SPI is an index based on the probability of recording a given amount of precipitation, and the probabilities are standardized so that an index of zero indicates the median precipitation amount (half of the historical precipitation amounts are below the median, and half are above the median). The index is negative for drought, and positive for wet conditions. As the dry or wet conditions become more severe, the index becomes more negative or positive (Ntale and Gan, 2003). SPI can also be used to determine the magnitude of a drought in a locality. Drought magnitude is the duration of drought with negative SPI deviation expressed in time period of month(s) (McKee *et al.*, 1993).

The two drought monitoring approaches, namely climate variable indices based and remote sensing based (satellite-derived vegetation indices (VIs)) were separately used in the past. Various studies have also demonstrated the relationships between climate variables (e.g., precipitation) and satellite-derived VIs (Di *et al.*, 1994; Ji and Peters, 2003). Even though there had been various efforts in the past to use meteorological point data or remotely sensed data, there were limited efforts to integrate these two approaches for practical drought monitoring to save drought victims. The main objective of this research is to characterize and identify drought incidence using both historic rainfall data and satellite images.

Materials and Methods

Study Area

The study area for this research is the whole of Ethiopia. Ethiopia occupies the interior of the Horn of Africa stretching between 3^0 and 14^0 N latitude and 33^0 and 48^0 E longitude, with a total area of 1.13 million km^2 (EMA, 1988).

Ethiopia is located in the tropics and variations in altitude have produced a variety of microclimates. Mean annual rainfall ranges from 2000 mm over some pocket areas in the southwest highlands, and less than 250 mm in the lowlands. In general, annual precipitation ranges from 800 to 2200 mm in the highlands (>1500 meters above sea level) and varies from less than 200 to 800 mm in the lowlands (<1500 meters above sea level). Rainfall also decreases northwards and eastwards from the high rainfall pocket area in the southwest (NMSA, 1996).

Data Sources and Analysis

For this study, historic rainfall (RF) data sets from the Ethiopian Meteorological Agency, and satellite images from Meteosat Second Generation (MSG) and National Oceanic and Atmospheric Administration (NOAA) AVHRR were used. To analyze the relationship between RF and NDVI values, data collected from 1982 through 2004 were used. Those

years were selected because we found complete data sets for both RF and imageries during those time periods.

There are over 600 rain gauge stations (Figure 1) found in Ethiopia that are classified into four different classes as synoptic, principal, 3rd, and 4th class stations (NMSA, 2001). For the correlation analysis between RF and NDVI, all of the four class stations were used. Average RF data from 1982 – 2004 were calculated for each 2 x 2 degree grids (Figure 3). For each of these grids one average RF value was calculated.

For the Standard Precipitation Index (SPI) analysis a total of 40 stations were selected. The spatial distributions of the selected stations are shown in Figure 2. For the remote sensing part, satellite images from MSG and NOAA AVHRR were used. From MSG 12 channels, we used channels 1 and 2 for detecting vegetation condition. These two visible channels are well known from similar channels to the AVHRR instruments that are on the NOAA satellites and can be used in combination to generate vegetation indices such as NDVI (EUMETSAT, 2005).

Figure 1. Distribution of meteorological stations in Ethiopia

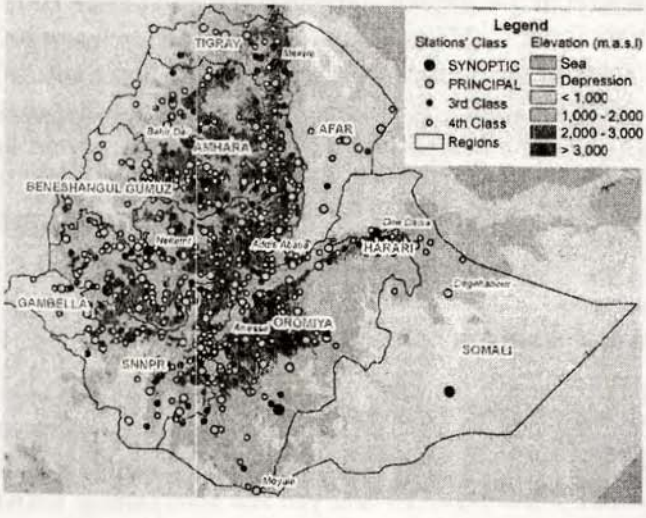

Source: Adapted from Ephrem and Meissner, 2010

Figure 2: Distribution of selected meteorological stations for SPI analysis

Source: Authors' Own Construction, 2010

Methods

Ethiopia is a country with heterogeneous ecosystem. This heterogeneity is mainly attributed to the variability in elevation and topography. This causes short distance variability and changes in both RF amount and distribution. The number of rain gauges in Ethiopia is small and unevenly distributed (Figure 1). Therefore, in this research for maximizing the homogeneity of the area and reducing the error due to scarcity of RF gauges in the country, we produced a total of twenty-one 2 x 2 degrees grid. The historical average RF gauge data and NOAA AVHRR NDVI data inside these grids were calculated. To observe the relationship between RF and NDVI, the RF recoded by all stations inside the grids were averaged from 1982 to 2004 and an average point data was generated. The same procedure was followed for the NOAA AVHRR NDVI values of the 2 x 2-degree grids. The correlation and scatter plots of these analyses are presented in Figure 6. The RF patterns inside these grids were also analyzed separately (Appendix 2). From this analysis different patterns were observed for different parts of the country. All the patterns observed are presented in Appendix 2.

The RF pattern analysis was done with the intent of maximizing homogeneity and control NDVI data for monitoring drought by comparing current NDVI with historical NDVI values. These historical average values of RF and NDVI are presented in Appendix 1.

Figure 3. Map of Ethiopia with 2 x 2 degree grids

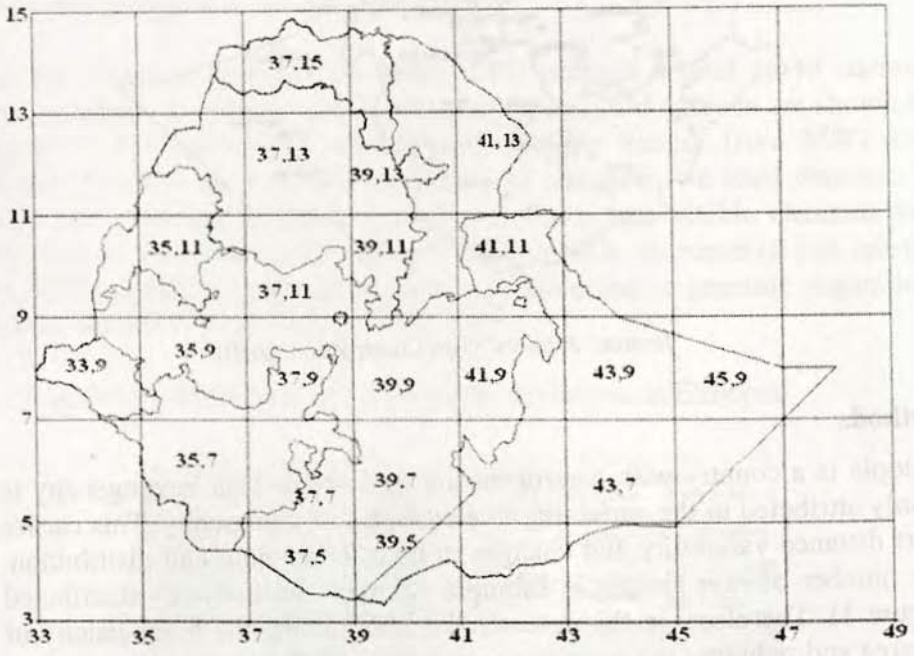

Source: Authors' Own Construction, 2010

SPI and Dev-NDVI for Monitoring Drought

Using the 40 selected stations (Figure 2), three-months SPI values were calculated for two time periods, 1984 and 2009. The three-month SPI was used because the three-month SPI calculated for October can use the precipitation total of August, September, and October, which are peak growing and/or maturity period of plants. This was also done with the

assumption that later on we can match the three-month SPI values with Dev_NDVI values. As a single numeric value, the SPI can be compared across regions with markedly different climates (Ntale and Gan, 2003). In this research, since the cumulative precipitation was not normally distributed, the data was transformed to a normal domain to standardize the drought index. Using the stations data (Figure 2), the three-month SPI was calculated using equation 1 (McKee et al., 1993). After getting these point data for the selected stations, ordinary kriging method was used for interpolating the values for the whole of Ethiopia.

$$SPI = \frac{P_i - P_{mean}}{s} \quad (1)$$

where SPI is the standard precipitation index, P_i is observed cumulative rainfall at a given time scale, P_{mean} is long-term mean rainfall of a given time period, and s is the standard deviation of the past rainfall record of a given time scale.

In the remote sensing imagery analysis part, ILWIS 3.6 software was used. The NDVI data from NOAA were used after preprocessing with the recommendation made by the data sources in the Meta Data details.

The 10-days images of MSG (1-10 October 2009) were imported to ILWIS raster image format using the "Multiple times in one file" option. This means that we had all 10 bands stacked (map list) together and made ready for the NDVI calculation. The raw data downloaded from MSG were pre-processed and the NDVI values were calculated using equation 2. During the analysis, cloud-contaminated pixels were removed from each individual image by examining the reflectance and temperatures. The daily NDVI values of MSG were aggregated on a dekadal basis. In a year, there are 36 dekads (one dekad is equal to 10 days).

The deviation of normalized difference vegetation index (Dev_NDVI) was calculated after processing the two datasets separately (NOAA historical NDVI and MSG NDVI data). Since the two data sources were found to have different resolutions, the MSG data was re-sampled to 8 km (to the

spatial resolution of NOAA AVHRR data). After importing the three-band image data to ILWIS 3.6 raster format, a script was written for calculating the Dev_NDVI.

Dev_NDVI is calculated using Equation 3.

$$NDVI = \frac{\rho_{nir} - \rho_{red}}{\rho_{nir} + \rho_{red}} \quad (2)$$

where ρ_{red} (0.4–0.7 mm) and ρ_{nir} (0.75–1.1 mm) are reflectance in red and near-infrared bands of the satellite images.

$$Dev\_NDVI = NDVI\_i - NDVI\_Mean\_i \quad (3)$$

where $NDVI\_i$ is the actual dekad (10-day composite) NDVI from MSG satellite and $NDVI\_Mean\_i$ is the long-term mean for the same-dekad NDVI from NOAA satellite.

Results and Discussions

Rainfall Pattern in Ethiopia

According to Verdin et al. (2005), the RF seasons for the country as a whole are March–May (locally called 'Belg'), and June–September (locally called 'Kiremt'). They also indicated that most of the rains in Ethiopia come in the period March to September, with a pause in many parts of the country around the end of May or beginning of June. The 'Belg' rains come in March–May, and the 'Kiremt' rains in June–September. A FEWS NET (2003) study also showed that April–May RF totals could explain 50% of the variance of long-cycle water requirement satisfaction index, revealing that this is a critical stage when rainfall deficits can negatively impact yields of crops harvested in September–December.

In our study, the overall monthly average RF pattern analysis showed that there is a difference between the different grids (Appendix 2). From this analysis, four major different patterns were identified. The first pattern is the one with high average RF during July and August. In this pattern, the rain starts in March with gradual increase and reaches the maximum in July

and August. This pattern is presented on Figure 4a using grid [35, 11]. The second pattern has high average RF during July and August and a secondary RF during March, April and May with highest average RF in April. This pattern is presented on Figure 4b using grid [41, 13]. The third pattern has high average RF during April and May and a secondary RF during September, October and November with highest average RF in April. This pattern is presented on Figure 4c using grid [39, 7]. The fourth pattern has RF throughout the year with relatively low average RF during December, January and February. This pattern is presented on Figure 4d using grid [35, 7]. The overall monthly average RF analysis for Ethiopia using the 21 grids is presented in Appendix 2 and the spatial distributions of the four RF patterns are also presented in Figure 5.

Results from both Verdin *et al.* (2005) and FEWS NET (2003) are not refined enough to develop a practical drought monitoring system in Ethiopia. Compared to these coarse classifications, our approach classified the country temporally and spatially (Figures 4 and 5). In our research we delineated the RF pattern in the country (Figure 5) and our aim was to develop a drought monitoring system specifically for the localities based on their RF patterns. The four patterns identified in this research are the basis for developing drought-monitoring system using the satellite data in our subsequent research.

Figure 4: Average RF for Ethiopia: pattern 1 (a), pattern 2 (b), pattern 3 (c) and pattern 4 (d)

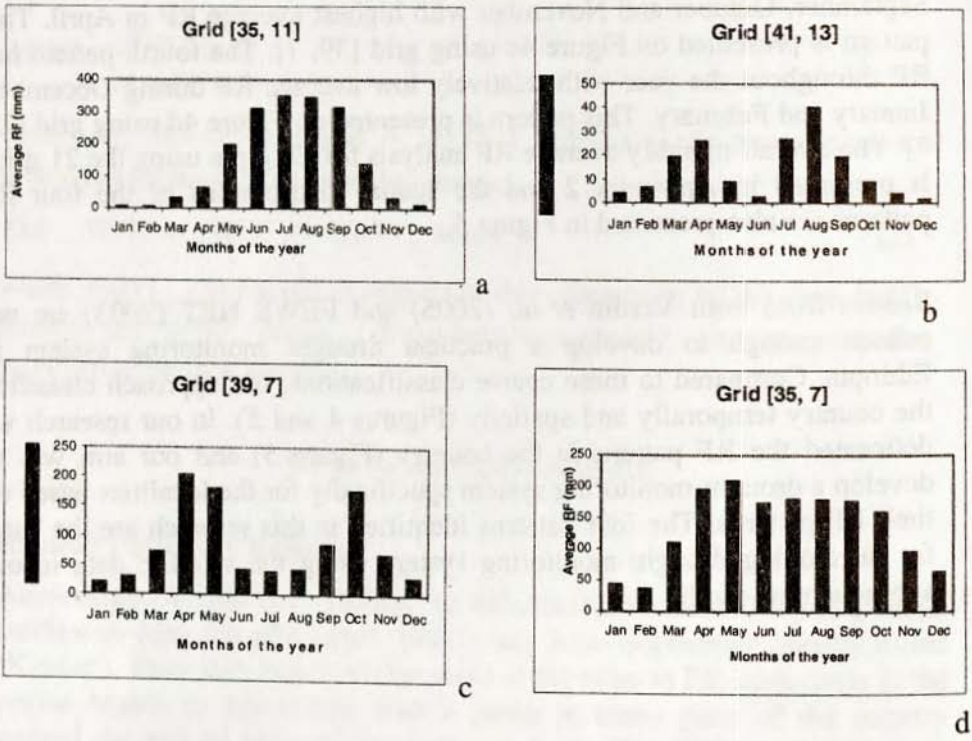

Source: Authors' Own Construction, 2010

Figure 5. The four average RF patterns using all RF gauges inside the 2 x 2 degree grids in Ethiopia, 1982 – 2004

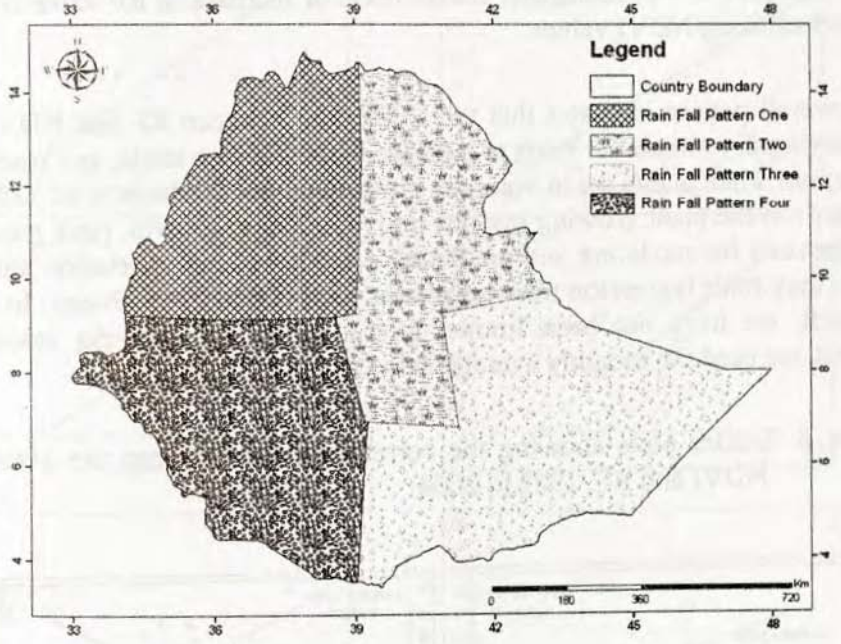

Source: Authors' Own Construction, 2010

Relationships between RF and NDVI

From the analysis of the relationship between average RF and average NDVI for 12 months, there were relatively high R^2 values for rainy months (Figure 6) as expected. For dry months, there were low relationships (with R^2 values of less than 0.5). The maximum R^2 values recorded were for May ($R^2 = 0.7613$) and September ($R^2 = 0.7698$) and the minimum values were in February ($R^2 = 0.2172$) and November ($R^2 = 0.2095$). The R^2 values showed a gradual increase from February to May, with a maximum value in May; it decreased in July, and then increased again in September (Figure 6).

The result showed that the main rainy months, which start in mid-June and end in mid-September, have strong relationship with NDVI values. From these analyses, it was found that the decrease or increase in RF value could be tracked using NDVI values.

The overall pattern indicates that the correlation between RF and NDVI is low during dry months. It starts to increase when the rain starts, and reaches maximum when plants are in vigorous growing stages. Tadesse *et al.* (2005) categorized the plant growing seasons into three (early growth, peak growth and harvest) for modeling and predicting drought related vegetation stress. Then, they built regression tree models for each of the three phases. In our research, we have not been limited to the vegetation growing seasons. Instead, we used the monthly average values throughout the year.

Figure 6: Scatter plots showing the correspondence between the average NDVI and RF, 1982 to 2004

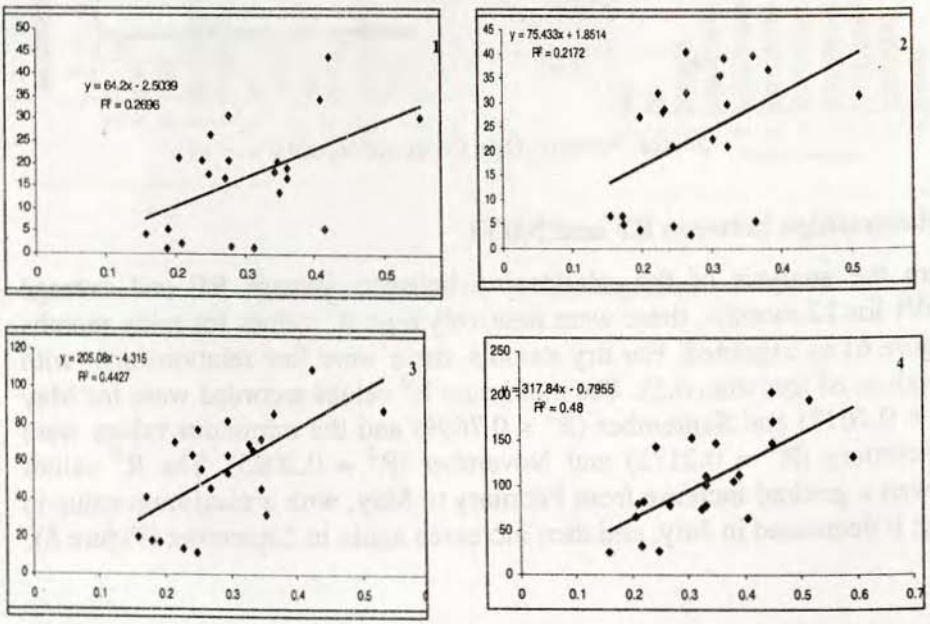

Figure 6… cont'd

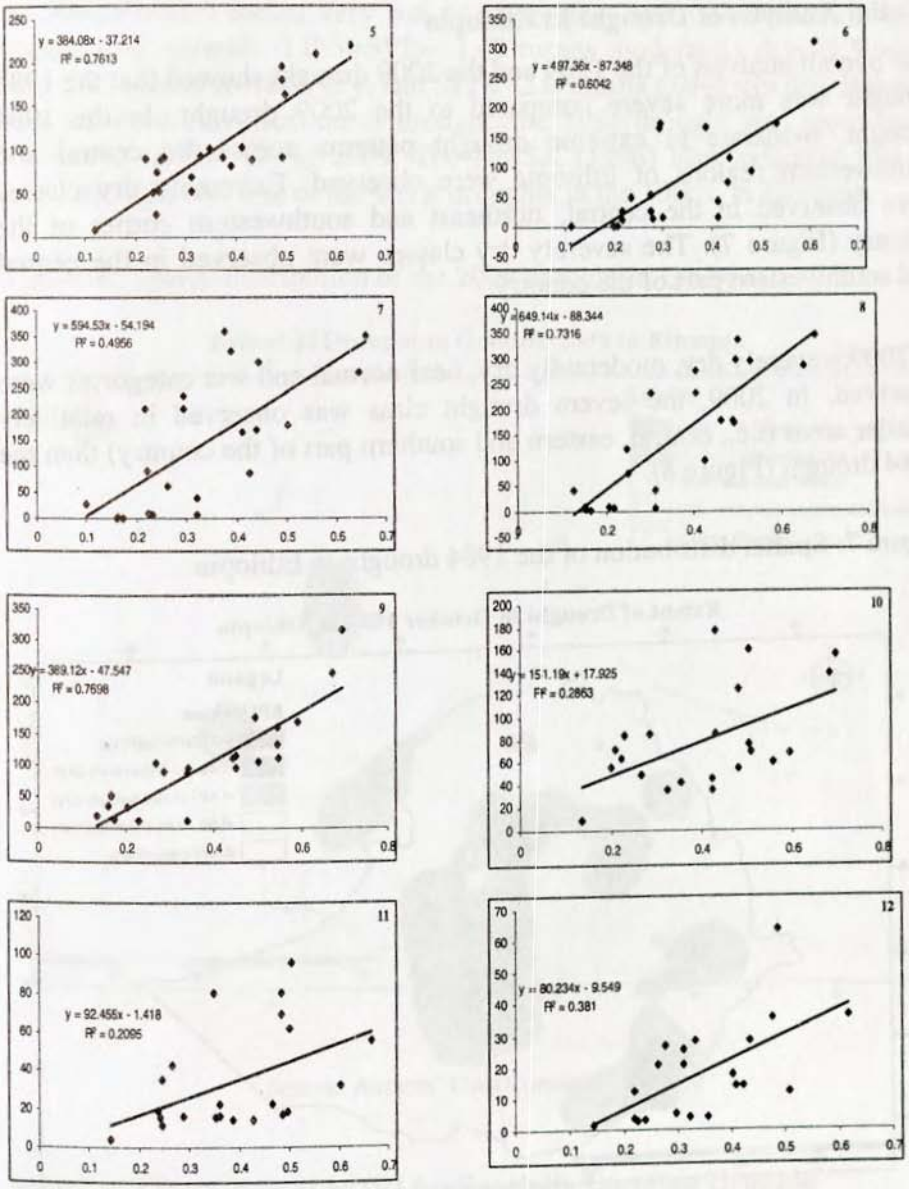

Source: Authors' Own Construction, 2010

NB. The numbers 1–12 correspond to January–December.

Spatial Analysis of Drought in Ethiopia

The overall analysis of the 1984 and the 2009 drought showed that the 1984 drought was more severe compared to the 2009 drought. In the 1984 drought, moderate to extreme drought patterns across the central and southwestern regions of Ethiopia were observed. Extremely dry classes were observed in the central, northeast and southwestern corner of the country (Figure 7). The severely dry classes were observed in the central and southwestern part of the country.

In 2009, severely dry, moderately dry, near normal and wet categories were observed. In 2009, the severe drought class was observed in relatively smaller areas (i.e., central, eastern and southern part of the country) than the 1984 drought (Figure 8).

Figure 7: Spatial distribution of the 1984 drought in Ethiopia

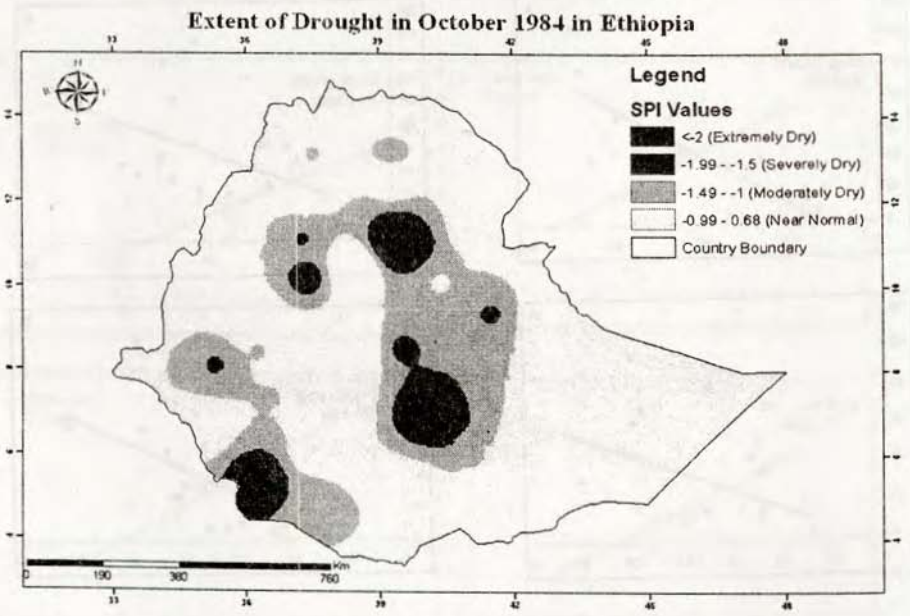

Source: Authors' Own Construction, 2010

According to McKee *et al.* (1993), SPI >=2 means extremely wet 1.99>=SPI>=1.0 means very wet or moderately wet; 0.99 >= SPI >=-0.99 means near normal; -1.0 >=SPI>=-1.49 means moderately dry; -1.5 >=SPI >= -1.99 means severely dry; and SPI < -2.0 means extremely dry. Based on this standard classification of drought, the 1984 drought was more severe compared to the one in 2009. The NMSA (1996) also indicated that the 1984 drought was one of the worst droughts in the 1980s, in Ethiopia.

Figure 8: Spatial distribution of the 2009 drought in Ethiopia

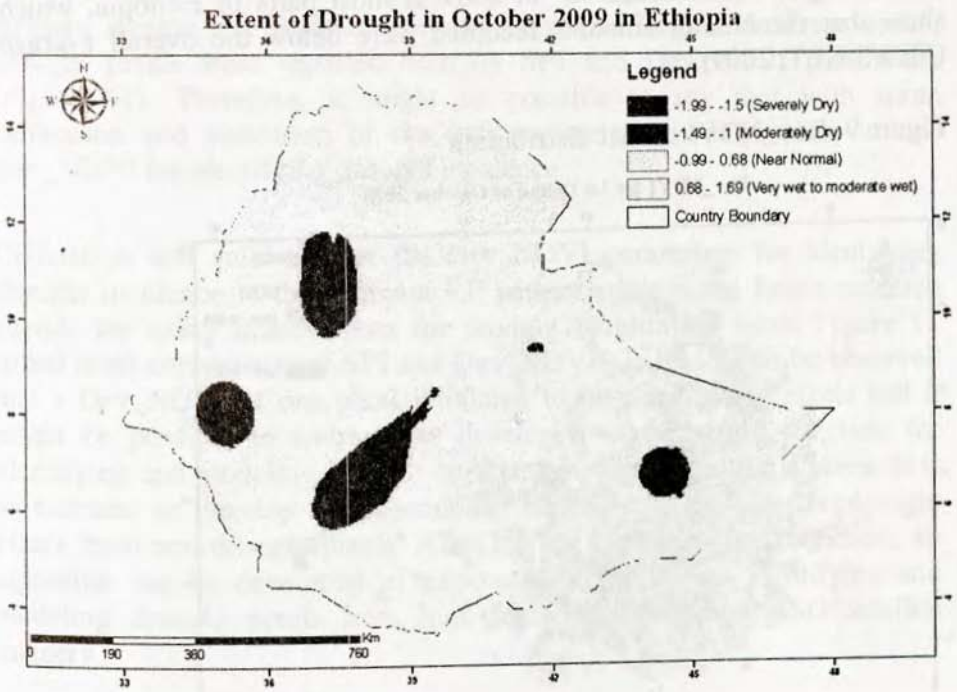

Source: Authors' Own Construction, 2010

NDVI and Deviation of NDVI for Spatially Locating Drought

In this section, we present the status of drought conditions in October 2009 using the NDVI parameter. This analysis was also primarily conducted with

the aim of testing the applicability of MSG data for spatio-temporal drought monitoring. The results were obtained by using first dekad of October 2009 MSG data and the long-term average NOAA AVHRR NDVI data.

The actual drought condition was determined by comparing the NDVI for the first dekad of October 2009 with the long-term mean NDVI using NOAA satellite data. Our results show that approximately 40% of the area exhibited negative deviation (see Figure 9). This indicates that drought conditions were observed in 2009 in different parts of Ethiopia. These results align with recorded RF in 2009 in most parts of Ethiopia, which show that the rainfall amounts recorded were below the overall average (FEWS NET, 2009).

Figure 9: Dev_NDVI spatial distribution

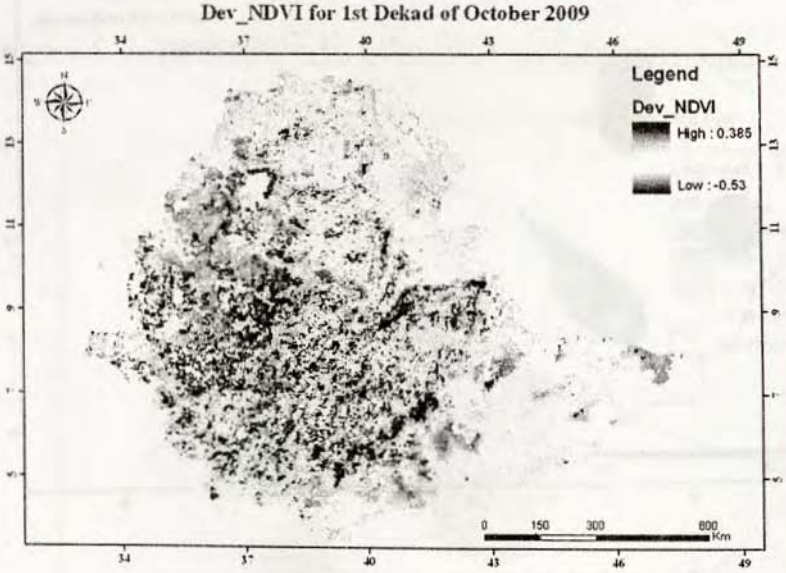

Source: Authors' Own Construction, 2010

The comparison of the SPI and Dev_NDVI maps also showed that there are some localities where similar patterns were observed. The two hot spots observed in the northwestern and western parts of Ethiopia from the SPI map were also observed in the Dev_NDVI analysis output map (Figure 10).

There is also a difference in the two maps in showing the intensity of drought. The SPI drought intensity shows the hot spots and the Dev_NDVI map shows the pixel level deviations. The Dev_NDVI drought intensity map is continuous compared to SPI map. This difference is attributed to the number of stations (only 40 stations) used for the SPI value interpolation.

From our analysis (pixel level comparison of SPI and Dev_NDVI), it can be observed that the drought identified as 'severely dry' in 2009 by SPI parameter (Figures 8) is related to high Dev_NDVI values (see Figure 10 and 11). Specifically, the two zones shown in Figure 10 are Awi Zone in Amhara Region and Agnuak Zone in Gambella Region. In these zones, drought pixels were reported both by SPI and Dev_NDVI parameters (Figure 11). Therefore, it might be possible to say that with some calibration and validation of the two parameters, it is possible to use Dev_NDVI for identifying drought incidence.

Calibration and validation of the Dev_NDVI parameters for identifying drought incidence in the different RF pattern areas is the future research agenda for using satellite data for drought monitoring. From Figure 11 (pixel level comparison of SPI and Dev_NDVI), it could also be observed that a Dev_NDVI of one pixel is related to its neighboring pixels and it might be possible to estimate or develop a mathematical function for identifying and modeling drought objects. The next step in this research is to estimate or develop a mathematical function to characterize drought pixels from non-drought pixels. After having the appropriate function, an algorithm can be developed to automate the process of identifying and modeling drought pixels from high temporal resolution MSG satellite imagery.

Figure 10: Comparison of SPI and Dev_NDVI maps, October 2009

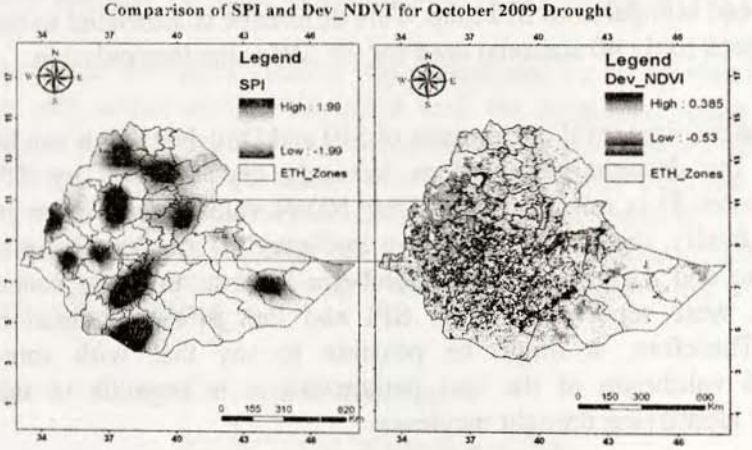

Source: Authors' Own Construction, 2010

NB. The arrows show a drought intensity using both SPI (left) and Dev_NDVI (right) parameters

Figure 11: Pixels level comparisons of SPI and Dev_NDVI.

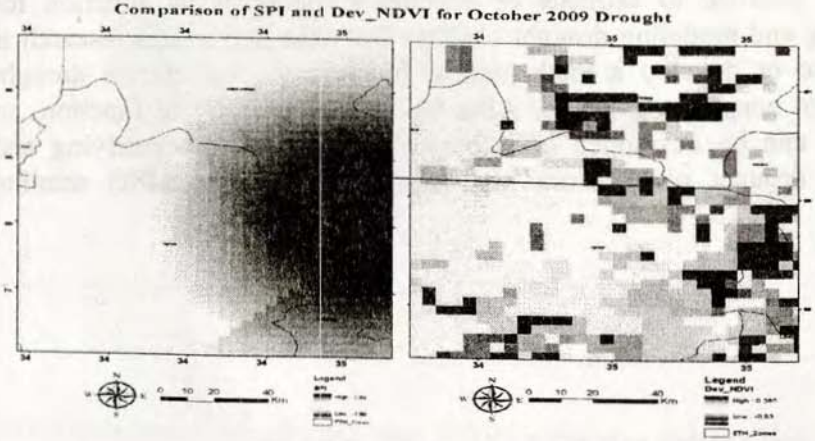

Source: Authors' Own Construction, 2010

NB. The arrow shows a drought intensity using both SPI and Dev_NDVI parameters during October 2009 in Gambela Region, Agnuak Zone.

Conclusions

The focus of this research was to characterize and identify drought incidences using both historic RF data and satellite images. NDVI and Dev_NDVI data from satellite sources were analyzed and compared with the historical RF records in forty stations. In this case the RF records were used as control parameters for the satellite source data. The relationship analysis between RF and NDVI showed that there are high R^2 values in the main rainy months. Overall, interesting results have been achieved in characterizing and identifying drought incidence using both historic RF data and satellite images data sources. Based on this study, it is possible to use the near-real time MSG and historical NOAA AVHRR NDVI and Dev_NDVI data with some calibration and validation to identify and predict drought incidence in advance and take appropriate actions for saving drought victims.

The results of this study may help decision makers to use advanced satellite technology for effective drought monitoring and early warning systems in various regions. Integrated with appropriate policies, these early warning systems can help to prevent famine and starvation in food-insecure regions. In the past, satellite technologies have primarily been used in areas of meteorological applications. In this research, the main emphasis is on mining knowledge (e.g., pattern recognition) from satellite images for drought hazard assessment and saving the lives of individuals who are affected by recurring droughts. The findings of this research can also assist decision makers in taking appropriate actions in time to save lives in drought-affected areas using advanced satellite technology.

Tadesse, T., Brown, J.F., Hayes, M.J.H. 2005. A new approach for predicting drought related vegetation stress: integrating satellite, climate, and biophysical data over the U.S. central plains. ISPRS Journal of Photogrammetry and Remote Sensing, 59(4), 244–253.

Tadesse, T., Haile, M., Senay, G., Brian, D., Cody, W., Knutson, L. 2008. The Need for Integration of Drought Monitoring Tools for Proactive Food Security Management in Sub-Saharan Africa. *Natural Resources Forum*, 32, 265–279.

UNCCD (United Nations Convention to Combat Desertification). 1999. Article 1, United Nations, Bonn, Germany.

UNEP (United Nations Environment Programme). 2006. Climate Change and Variability in the Sahel Region: Impacts and Adaptation Strategies in the Agricultural Sector, http://www.unep.org/Themes/Freshwater/Documents/pdf/ClimateChangeSahelCombine.pdf, Accessed on July 12, 2010.

Ungani, L. and Kogan, F. 1998. Drought monitoring and corn yield estimation in southern Africa from AVHRR data. *Remote Sensing of Environment*, 63, 219 -232.

UNISDR (United Nations secretariat of the International Strategy for Disaster Reduction). 2009. Drought Risk Reduction Framework and Practices: Contributing to the Implementation of the Hyogo Framework for Action, Geneva, Switzerland.

Verdin, J., Funk, C., Senay, G., Choularton, R. 2005. Climate science and famine early warning. *Philosophical Transactions*, 360, 2155–2168.

Wilhite, D. A. 2005. *Drought andWater Crisis: Science, Technology and Management Issues.* London: Taylor & Francis Group.

Appendices

Appendix 1: Average monthly RF (MM) and NDVI data from 1982–2004

Grids	Items measured for the grids	Months of the year											
		Jan	Feb	Mar	Apr	May	Jun	Jul	Aug	Sep	Oct	Nov	Dec
37,15	Average RF	1.82	4.68	13.74	33.22	89.11	165.87	321.11	296.58	132.95	53.99	14.50	3.87
	Average NDVI	0.28	0.25	0.23	0.22	0.22	0.29	0.39	0.50	0.54	0.48	0.39	0.32
37,13	Average RF	1.52	2.74	11.40	27.22	73.24	173.30	359.76	335.97	161.18	75.71	14.40	3.80
	Average NDVI	0.31	0.27	0.25	0.25	0.24	0.30	0.38	0.50	0.55	0.51	0.43	0.36
39,13	Average RF	20.67	31.96	63.35	77.43	52.81	25.86	211.84	231.38	94.81	34.81	16.34	20.55
	Average NDVI	0.24	0.23	0.24	0.27	0.25	0.22	0.22	0.30	0.34	0.32	0.29	0.26
41,13	Average RF	4.13	6.54	19.50	25.93	8.51	2.24	26.27	40.04	19.34	8.78	3.97	1.58
	Average NDVI	0.16	0.16	0.16	0.16	0.12	0.11	0.10	0.13	0.13	0.13	0.14	0.14
35,11	Average RF	5.72	5.59	32.31	63.94	196.36	311.71	350.32	345.69	315.76	138.25	32.18	11.93
	Average NDVI	0.41	0.36	0.35	0.40	0.49	0.61	0.66	0.68	0.70	0.68	0.60	0.51
37,11	Average RF	13.65	22.47	53.97	73.84	101.42	166.72	299.30	294.83	169.15	68.61	18.34	13.82
	Average NDVI	0.35	0.30	0.29	0.32	0.35	0.39	0.44	0.53	0.59	0.60	0.50	0.42
39,11	Average RF	30.81	40.49	81.50	100.34	68.61	54.08	237.48	275.39	115.69	45.21	22.73	25.29

Appendix 1 ... cont'd

	Average NDVI	0.28	0.27	0.30	0.33	0.31	0.28	0.29	0.40	0.45	0.42	0.36	0.31
41,11	Average RF	21.17	27.15	70.53	143.35	87.59	49.72	91.31	121.92	102.84	48.47	15.58	12.49
	Average NDVI	0.21	0.20	0.21	0.24	0.25	0.23	0.22	0.25	0.27	0.27	0.24	0.22
33,9	Average RF	20.67	31.96	63.35	77.43	52.81	25.86	211.84	231.38	94.81	34.81	16.34	20.55
	Average NDVI	0.36	0.32	0.35	0.45	0.49	0.41	0.32	0.31	0.34	0.43	0.48	0.43
35,9	Average RF	30.37	31.40	87.92	131.40	220.32	273.55	279.94	284.99	247.47	155.88	55.51	36.34
	Average NDVI	0.55	0.51	0.53	0.59	0.63	0.66	0.64	0.65	0.67	0.70	0.67	0.62
37,9	Average RF	20.33	39.23	66.44	104.51	101.60	115.02	170.32	174.60	110.88	60.76	17.16	13.80
	Average NDVI	0.35	0.32	0.33	0.38	0.41	0.44	0.44	0.49	0.55	0.56	0.48	0.41
39,9	Average RF	18.18	35.55	69.24	112.70	88.54	73.76	166.02	178.17	106.32	68.98	22.45	17.65
	Average NDVI	0.34	0.31	0.33	0.39	0.43	0.43	0.41	0.46	0.50	0.51	0.47	0.40
41,9	Average RF	17.67	28.12	55.74	110.92	81.16	54.44	62.24	72.49	88.60	42.55	15.35	5.16
	Average NDVI	0.25	0.23	0.26	0.33	0.39	0.33	0.26	0.25	0.29	0.35	0.35	0.30
43,9	Average RF	5.38	4.80	18.03	82.56	90.88	11.33	3.02	8.26	51.37	63.18	11.80	3.62
	Average NDVI	0.19	0.17	0.18	0.22	0.26	0.22	0.16	0.15	0.17	0.22	0.24	0.22
45,9	Average RF	2.41	3.91	17.02	79.33	50.83	1.23	0.32	0.45	13.55	71.19	35.77	3.31

Appendix 1 … cont'd

	Average NDVI	0.21	0.20	0.19	0.21	0.23	0.21	0.17	0.16	0.17	0.21	0.25	0.24
35,7	Average RF	43.67	36.70	110.03	195.73	209.59	173.94	180.33	179.29	177.06	160.15	96.05	63.60
	Average NDVI	0.42	0.38	0.42	0.52	0.56	0.53	0.50	0.49	0.49	0.50	0.50	0.49
37,7	Average RF	34.34	39.63	85.75	171.26	163.37	92.19	87.17	100.26	111.02	124.95	62.03	35.37
	Average NDVI	0.41	0.36	0.37	0.45	0.50	0.48	0.43	0.43	0.44	0.48	0.50	0.48
39,7	Average RF	19.10	29.69	72.54	204.01	180.20	43.35	39.28	41.34	86.56	177.13	69.64	28.38
	Average NDVI	0.36	0.32	0.35	0.45	0.49	0.41	0.32	0.31	0.34	0.43	0.48	0.43
43,7	Average RF	1.14	6.77	40.90	64.84	25.53	1.59	0.26	3.01	36.07	56.18	19.12	2.89
	Average NDVI	0.19	0.17	0.17	0.21	0.24	0.20	0.16	0.15	0.16	0.20	0.24	0.22
37,5	Average RF	26.48	28.59	77.32	153.45	91.70	13.56	10.03	7.70	34.74	84.38	42.74	26.75
	Average NDVI	0.25	0.23	0.25	0.31	0.33	0.28	0.22	0.21	0.20	0.23	0.27	0.28
39,5	Average RF	16.88	21.07	45.56	147.15	91.37	17.33	7.63	5.42	12.76	85.44	80.21	28.07
	Average NDVI	0.27	0.25	0.27	0.35	0.37	0.30	0.23	0.22	0.23	0.28	0.35	0.33

Source: Authors' Own Construction, 2010

Appendix 2: Rain fall pattern for the 2 x 2 degree grids

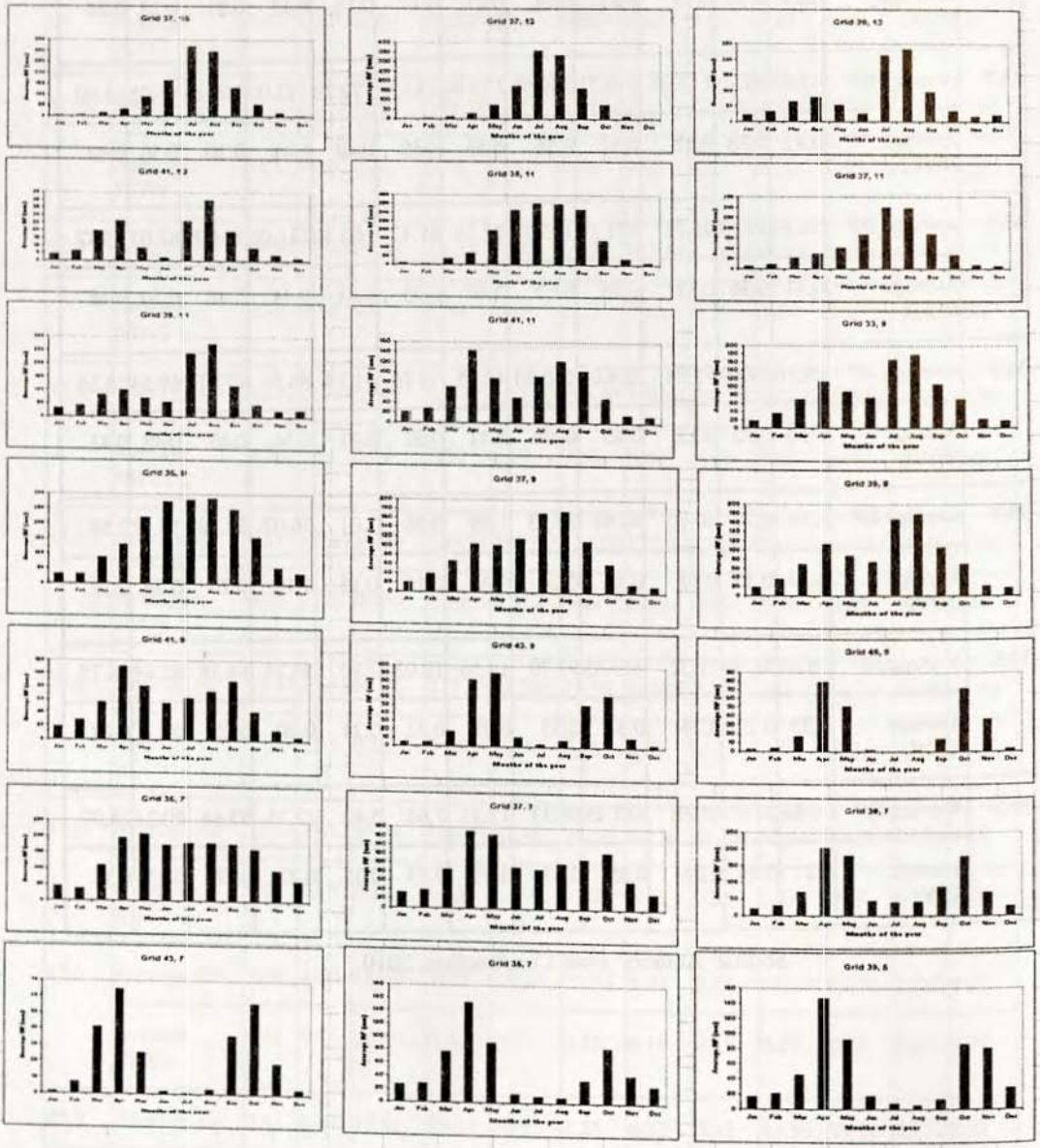

Source: Authors' Own Construction, 2010